Thermal Conductivity of Individual Single-Wall Carbon Nanotubes

Jennifer R. Lukes
e-mail: jrlukes@seas.upenn.edu

Hongliang Zhong

Department of Mechanical Engineering and
Applied Mechanics,
University of Pennsylvania,
Philadelphia, PA 19104

Despite the significant amount of research on carbon nanotubes, the thermal conductivity of individual single-wall carbon nanotubes has not been well established. To date only a few groups have reported experimental data for these molecules. Existing molecular dynamics simulation results range from several hundred to 6600 W/m K and existing theoretical predictions range from several dozens to 9500 W/m K. To clarify the several-order-of-magnitude discrepancy in the literature, this paper utilizes molecular dynamics simulation to systematically examine the thermal conductivity of several individual (10, 10) single-wall carbon nanotubes as a function of length, temperature, boundary conditions and molecular dynamics simulation methodology. Nanotube lengths ranging from 5 nm to 40 nm are investigated. The results indicate that thermal conductivity increases with nanotube length, varying from about 10 W/m to 375 W/m K depending on the various simulation conditions. Phonon decay times on the order of hundreds of fs are computed. These times increase linearly with length, indicating ballistic transport in the nanotubes. A simple estimate of speed of sound, which does not require involved calculation of dispersion relations, is presented based on the heat current autocorrelation decay. Agreement with the majority of theoretical/computational literature thermal conductivity data is achieved for the nanotube lengths treated here. Discrepancies in thermal conductivity magnitude with experimental data are primarily attributed to length effects, although simulation methodology, stress, and intermolecular potential may also play a role. Quantum correction of the calculated results reveals thermal conductivity temperature dependence in qualitative agreement with experimental data.
[DOI: 10.1115/1.2717242]

Keywords: thermal conductivity, molecular dynamics simulation, phonon, single-wall carbon nanotube

Introduction

Recent advances in micro- and nanofabrication have enabled the continuing reduction in size of electronic devices. Smaller sizes have led to higher device densities at the expense of increased power demand and the resultant heat generation. New thermal management strategies are thus critically important to continued high performance, reliability, and lifetime. One such strategy is to develop novel high thermal conductivity materials based on carbon nanotubes. Carbon nanotubes, which come in single- and multiwall forms, are rolled up from graphene sheets into cylinders. Early work predicted superior thermal conductivity, exceeding even that of diamond, for carbon nanotubes [1]. Most measurements on nanotube materials indicate that thermal conductivity increases monotonically with increasing temperature even above ambient temperature. Two groups have observed experimental thermal conductivity values of more than 3000 W/m K at room temperature for individual multiwall nanotubes (MWNTs), although the tube diameters are slightly different: 14 nm from Kim et al. [2] and 16.1 nm from Fujii et al. [3]. Choi et al. found a much lower value of 300 W/m K for MWNTs with 20 nm outer diameter and 1.4 μm length at room temperature [4]. Hone et al. [1] found that the thermal conductivity of aligned single-wall nanotube (SWNT) crystalline ropes is about 250 W/m K at 300 K and estimated that the longitudinal thermal conductivity of a single SWNT ranges from 1750 W/m K to 5800 W/m K. The first thermal conductance measurement on an isolated SWNT revealed a higher room-temperature thermal conductivity than that of MWNT, ranging from 2000 W/m K to 10000 W/m K depending on the diameter assumed in the conversion from conductance to conductivity [5]. More recent measurements, carried out above room temperature on a 2.6 μm long single wall carbon nanotube, display a peak thermal conductivity value of about 3400 W/m K near 300 K, decreasing to about 1200 W/m K at 800 K [6]. Within the above results (Table 1), there is significant variation in the data for nanotubes of varying diameters and lengths.

Molecular Dynamics Simulation Techniques. Molecular dynamics (MD) simulation [7] provides another approach for determining the thermal conductivity of carbon nanotubes, and yields additional atomistic information useful for analyzing thermal energy transport in SWNT and other carbon nanotube based materials. Classical MD involves integration of Newton's equations of motion for atoms interacting with each other through an empirical interatomic potential. It does not explicitly model electrons and therefore cannot simulate electron–electron or electron–phonon interactions. The phonon contribution for thermal conductivity is dominant in both MWNTs and SWNTs at all temperatures [8–10], which justifies neglecting electronic effects in simulations of carbon nanotubes.

In general there are three ways to compute the thermal conductivity in a solid. Nonequilibrium molecular dynamics (NEMD) [11] is based on Fourier's law, which relates the heat current in the axial direction to the axial temperature gradient through thermal conductivity

Table 1 Thermal conductivity of isolated single-wall carbon nanotubes at $T_{MD}=300$ K

	k (W/m K)	Tube length (nm)	Cross-sectional area (m^2)	Chirality	Simulation technique
Molecular dynamics simulation					
Berber et al. [16]	6600	2.5	29×10^{-19}	(10, 10)	HNEMD
Osman et al. [17]	1700	30	14.6×10^{-19}	(10, 10)	NEMD
Che et al. [18]	2980	40	4.3×10^{-19}	(10, 10)	EMD
Yao et al. [19]	$1 - 4 \times 10^{23}$	6–60	14.6×10^{-19}	(10, 10)	EMD
Padgett and Brenner [20]	40–320	20–310	14.6×10^{-19}	(10, 10)	NEMD
Moreland et al. [21]	215–831	50–1000	14.6×10^{-19}	(10, 10)	NEMD
Maruyama [22]	260–400	10–400	14.6×10^{-19}	(10, 10)	NEMD
Boltzmann–Peierls phonon transport equation (316 K)					
Mingo and Broido [24]	80–9500	$10-10^9$		(10,0)	

	k (W/m K)	Tube length (nm)	Diameter (nm)
Experimental measurement[a]			
Kim et al. [2] (MWNT)	3000	2500	14
Fujii et al. [3] (MWNT)	500	3600	28.2
	1800	1890	16.1
	2800	3700	9.8
Yu et al. [5]	2000	2600	1
	10,000	2600	3
Pop et al. [6]	3400	2600	1.7
Choi et al. [4] (MWNT)	300	1400	20

[a]Chirality unknown.

$$J_z = q_z V = -kV\frac{dT}{dz} \quad (1)$$

Equilibrium molecular dynamics (EMD) [12] is based on the Green–Kubo formula derived from linear response theory [13]. Simplifying for the case of axial conduction yields the thermal conductivity expression

$$k = \frac{1}{Vk_BT^2}\int_0^\infty \langle J_z(0)J_z(t)\rangle dt \quad (2)$$

where J_z is the axial component of the heat current $\vec{J}$ [14]

$$\vec{J}(t) = \sum_i \vec{v_i}\varepsilon_i + \frac{1}{2}\sum_{ij, i\neq j} \vec{r_{ij}}(\vec{f_{ij}}\cdot\vec{v_i}) \quad (3)$$

and the term inside the angle brackets in Eq. (2) represents the axial heat current autocorrelation function (HCACF). The temporal decay of the average HCACF represents the time scale of thermal transport.

The third method, homogeneous NEMD (HNEMD) [15], is a nonequilibrium approach in which an external field is applied to the system to represent the effects of heat flow without physically imposing a temperature gradient or flux. $\vec{F_e}$ is the external field that adds an extra force $\Delta\vec{F_i}$ to each individual atom by

$$\Delta\vec{F_i} = (\varepsilon_i - \langle\varepsilon\rangle)\vec{F_e} - \sum_{j(\neq i)} \vec{f_{ij}}(\vec{r_{ij}}\cdot\vec{F_e}) + \frac{1}{N}\sum_{jk(j\neq k)} \vec{f_{jk}}(\vec{r_{jk}}\cdot\vec{F_e}) \quad (4)$$

Extrapolating to zero external field [15] and applying $\vec{F_e}$ in the axial direction allows the thermal conductivity to be determined from

$$k = \lim_{F_e\to 0}\lim_{t\to\infty} \frac{\langle J_z(\vec{F_e},t)\rangle}{F_e TV} \quad (5)$$

where the axial heat current is time averaged. This method is computationally efficient, but the extrapolation to zero $\vec{F_e}$ can be a challenge as is shown later.

Previous Modeling Work. Several classical MD simulations have been performed in order to pinpoint the thermal conductivity of isolated (10, 10) SWNT [16–22]. Table 1 lists these results. It is seen that the values vary from several hundred to 6600 W/m K, with one outlier point [19] estimated at 10^{23} W/m K! In general, most values are lower than experimental data [5,6]. As the structural details of the tubes measured in the experiments are not known, it is difficult to compare to simulations on specific tube chiralities. There is still significant uncertainty as to the correct value of SWNT thermal conductivity.

Berber et al. [16] found that thermal conductivity increases with increasing temperature, reaches a peak at around 100 K, and finally decreases to about 6600 W/m K at room temperature. Osman et al. [17] found a similar behavior with a peak of near 400 K and a conductivity of about 1700 W/m K at 300 K. Che et al. [18] claimed to find length convergent thermal conductivity of about 2980 W/m K for a 40 nm long tube at room temperature. Yao et al. [19] calculated thermal conductance of carbon nanotubes; a conversion to conductivity by dividing thermal conductance by cross-sectional area gives results 23 orders of magnitude higher than other literature values. Additionally their phonon spectra appear quite different from those of other MD simulations [17,22]. The reason for those extreme values might be the violation of the ballistic upper bound to thermal conductivity pointed out by Mingo and Broido [23]. Padgett and Brenner [20] predicted thermal conductivity about 160 W/m K at 300 K, and Moreland et al. [21] found that the thermal conductivity at 300 K increases

from 215 W/m K at 50 nm to 831 W/m K at 1000 nm tube length. Maruyama [22] showed that the thermal conductivity is around 400 W/m K for a 400 nm long tube and increases steadily with length with an exponent of 0.15. In the latter two results, length convergence is still not achieved even for the longest nanotubes simulated. Mingo and Broido [24] solved the linearized Boltzmann–Peierls phonon transport equation by considering three-phonon scattering processes to higher order and showed that at short lengths the thermal conductivity increases with length (ballistic regime) while at longer lengths (diffusive regime) a length convergent value is achieved. The thermal conductivity of individual 100 nm long (10, 0) SWNT at 316 K was about 100 W/m K, and the length convergent value is as high as about 9500 W/m K.

Possible Reasons for Literature Discrepancies. As discussed above, nanotube length is a significant reason for the discrepancies in the literature. Various groups have performed calculations and measurements at different lengths and thus at different locations in the ballistic-diffusive continuum, so the observed length dependence is not surprising in light of these observations. Temperature effects are also important, as indicated by the peaking behavior observed by several authors [5,16,17]. Another reason for these discrepancies arises from differing choices for the nanotube cross-sectional area. In Eqs. (1), (2), and (5) it is evident that thermal conductivity is inversely proportional to nanotube volume, which is equal to cross-sectional area multiplied by nanotube length. The choice of nanotube area thus influences the calculated thermal conductivity value, and to compare obtained thermal conductivities from different groups it is imperative to scale all values by the same area. Berber et al. [16] calculated the area based upon the fact that tubes have an interwall separation of about 3.4 Å in nanotube bundles. Che et al. [18] chose a ring of 1 Å thickness for the cross-sectional area as the geometric configuration, while Maruyama [22] used a ring of van der Waals thickness of 3.4 Å. The rest [17,19–21] calculated the area as a circle with circumference defined by the centers of the atoms around the nanotube. Scaling all tubes by the same area still does not eliminate the differences. All of the above studies except for one used the Tersoff–Brenner (TB) bond order potential [25] to model the carbon nanotubes. Padgett and Brenner [20] used the reactive bond order potential (REBO) [26], an improved second-generation version of the TB potential, in an NEMD simulation. They found a thermal conductivity of 160 W/m K at 61.5 nm nanotube length. Moreland et al. [21] and Maruyama [22], who also used NEMD, employed the TB potential and found somewhat higher values: 215 W/m K at 50 nm length and 321 W/m K at 20 nm length, respectively. These differences may be partially caused by the slightly different form of the potential used.

Stress in the nanotubes may also contribute to the discrepancies. Moreland et al. [21] determined the stress-free tube length by running simulations with free boundaries at the tube ends to allow for longitudinal expansion/contraction, and then applied periodic boundary conditions (PBCs) for the remainder of the simulations. They found much lower thermal conductivity than that from experiments and from some of the papers above. As no mention of efforts to mitigate stress by relaxing the structure is discussed in these other papers, it is possible that some of the high calculated values [16–19] may be caused by compression of the tubes. Stress/strain effects have already been demonstrated to be important in other nanostructures [27]. The stress state of the experimental measurements is unknown.

It is not clear whether EMD or NEMD is better for simulating SWNT [21]. Also, the choice of axial boundary condition influences the thermal transport. The phonon mean free path in SWNT is several microns [28], and for nanotubes shorter than this length phonon scattering from free boundaries will be important. Nanotubes modeled with periodic boundary conditions have no free boundary and thus boundary scattering is eliminated, leaving

phonon–phonon interactions as the only scattering mechanism. For a finite-length tube in which the phonons are scattered at the ends, it is more physically meaningful to use free boundary conditions in the simulations.

To clarify the correct temperature and length dependence of individual (10, 10) SWNTs, this paper investigates the effects of boundary conditions and MD simulation methods under a consistent set of cross-sectional areas, potentials, and stress conditions. Phonon density of states and phonon relaxation times are also calculated to better understand phonon modes and phonon scattering. Although the study of thermal conductance rather than thermal conductivity may be more appropriate in systems like carbon nanotubes that experience ballistic transport, thermal conductivity is investigated here for ease of comparison to available literature data.

Computational Procedure

In order to study the temperature and length dependence of thermal conductivity, four different (10, 10) SWNTs are investigated using classical MD. They have 800, 1600, 3200, and 6400 atoms corresponding to nanotube lengths of about 5 nm, 10 nm, 20 nm, and 40 nm, respectively. The temperature ranges from 100 K to 500 K. The initial configuration of (10, 10) SWNT is constructed using a bond length of 1.42 Å. To study the effect of different boundary conditions, both free boundary and PBC are used. In PBC simulations, an extra simulation is run first with free boundaries to obtain the stress-free tube length. This length is typically very close to the original starting length.

To model the bonded carbon–carbon interactions, the REBO potential is used [26]. The nonbonded interactions between atoms are modeled using the Lennard-Jones potential. The total initial linear and angular momenta are removed once at the beginning of the simulation by subtracting the linear and angular velocity components [29]

$$\vec{v}_i\big|_{\text{new}} = \vec{v}_i\big|_{\text{old}} - \sum_j \frac{\vec{v}_j\big|_{\text{old}}}{N} - \vec{\omega} \times \vec{r}_i \qquad (6)$$

This procedure ensures that the isolated carbon nanotube does not have translational or rotational movement, which simplifies the calculation of the heat current along the tube axis. In all simulations, a 3.4 Å thickness cylinder is chosen as the geometric configuration. Zero linear and angular momenta are well conserved at all time steps. Details on the calculation of the instantaneous angular velocity of the system can be found in Ref. [30]. The resulting velocities are scaled to match the initial temperature. The time step is 1 fs for all cases. For the first 40 ps a constant temperature simulation with the Nosé–Hoover thermostat [31] is used to equilibrate the system to the desired temperature. Then a 400 ps long simulation is performed in the microcanonical ensemble to compute the heat current along the tube axis. The HCACF is calculated up to 200 ps, after which time it has decayed to approximately zero.

To calculate thermal conductivity using EMD it is necessary to integrate the HCACF (Eq. (2)). If PBCs are used, phonons will reenter the simulation box and interfere with themselves at times longer than the time a phonon takes to ballistically traverse the nanotube, τ_b, resulting in spurious self-correlation effects in the HCACF [32]. This time is estimated conservatively as the nanotube length L divided by the speed of sound of the longitudinal acoustic mode c_{LA}, which, at 20 km/s [8], is the fastest traveling mode in the nanotube. To avoid these spurious effects, a best fit curve to the HCACF decay is found for $t < \tau_b$ ("early time").

As suggested by Che et al. [33], the decay is fitted by a double exponential function

$$\text{HCACF} = A_1 \exp(-t/\tau_1) + A_2 \exp(-t/\tau_2) \qquad (7)$$

where τ_1 and τ_2 are time constants associated with fast and slow decays, respectively. Physically τ_1 and τ_2 are interpreted as half of
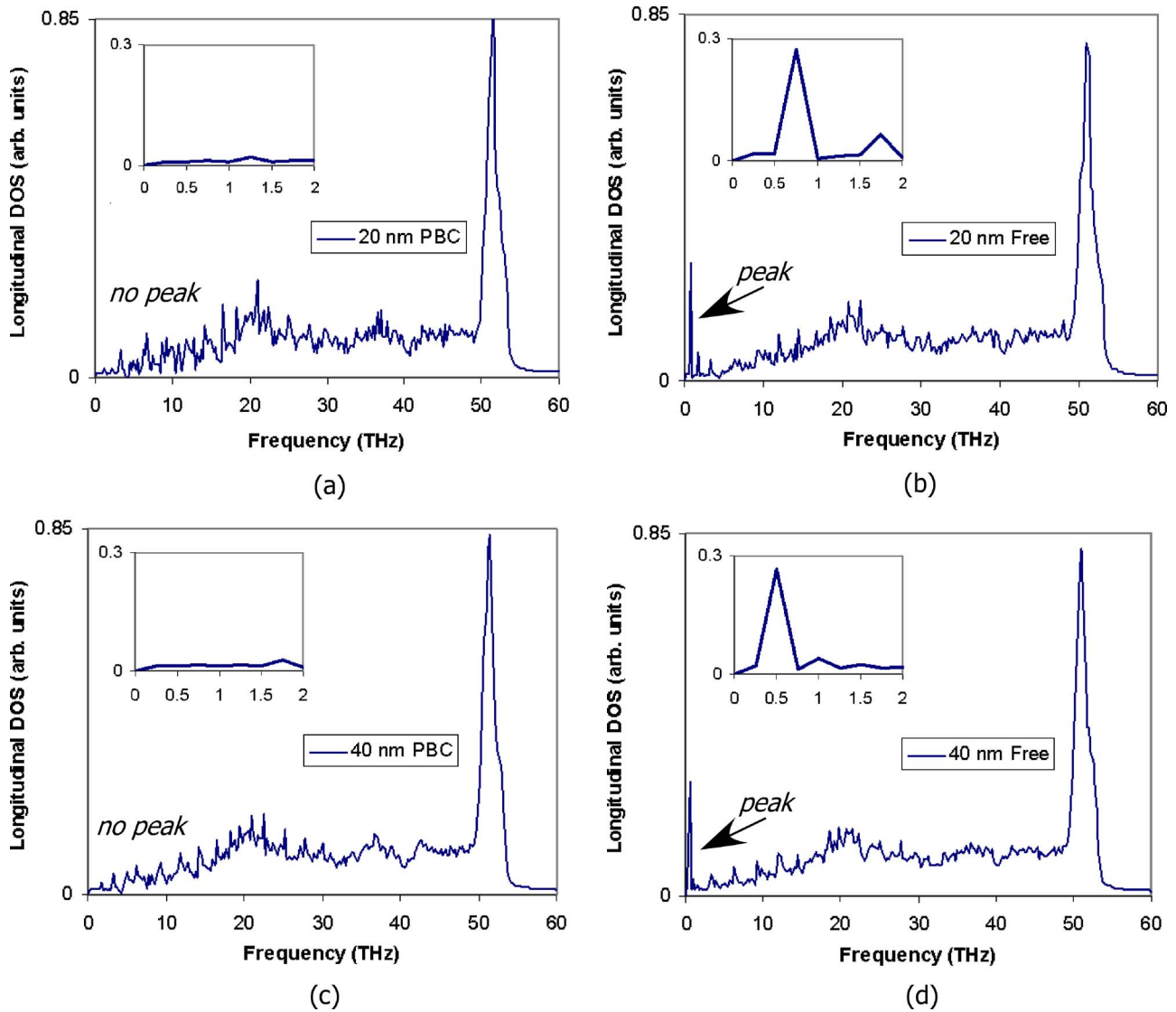
Fig. 1 Longitudinal phonon density of states at $T_{MD}=300$ K for $(10, 10)$ SWNTs with different lengths and boundary conditions: (a) 20 nm periodic; (b) 20 nm free; (c) 40 nm periodic; and (d) 40 nm free

the period for energy transfer between two neighboring atoms or the "local" time decay, and as the average phonon–phonon scattering time, respectively [34]. Thermal conductivity is then computed analytically by integrating Eq. (7) from $t=0$ to ∞ using the best fit τ_1 and τ_2 values. In each simulation, the general expression for error propagation [35] is used to calculate the probable error of thermal conductivity

$$\sigma_k = \sqrt{\sigma_T^2 \left(\frac{\partial k}{\partial T}\right)^2 + \sigma_{(\langle J_z(t)J_z(0)\rangle)}^2 \left(\frac{\partial k}{\partial \langle J_z(t)J_z(0)\rangle}\right)^2} \qquad (8)$$

Because thermal expansion of the tube is negligible [36], variation of the tube volume is not included in the error estimation. The standard error of the HCACF depends on the simulation run time t_{run} and the correlation time t_{corr} [37]

$$\sigma_{\langle J_z(t)J_z(0)\rangle} = \sqrt{\frac{2t_{corr}}{t_{run}}}\langle J_z^2\rangle \qquad (9)$$

where the correlation time is defined by

$$t_{corr} = \frac{2\int_0^\infty dt\ \langle J_z(t)J_z(0)\rangle^2}{\langle J_z^2\rangle^2} \qquad (10)$$

Results and Discussion

Phonon Density of States. Thermal properties strongly depend on the phonon density of states (DOS) which is the number of vibrational states per unit frequency. In MD simulations, the longitudinal DOS is calculated as

$$D_{long}(\omega) = S \int dt\ e^{-i\omega t}\langle v_z(t)v_z(0)\rangle = S\Delta t \cdot \text{FFT}[\langle v_z(t)v_z(0)\rangle] \qquad (11)$$

where the product of the scale factor $S=Nm/k_B T_{MD}$, the MD simulation timestep Δt, and the fast Fourier transform of the averaged axial velocity autocorrelation function is taken. Often in MD studies the DOS is plotted in arbitrary units rather than units of states per unit frequency; typically this is done by neglecting
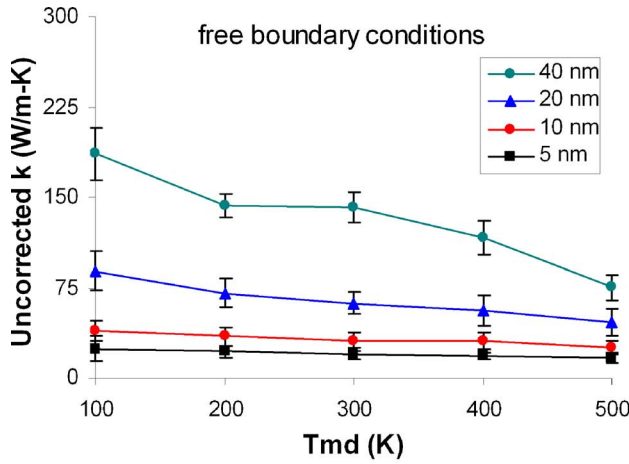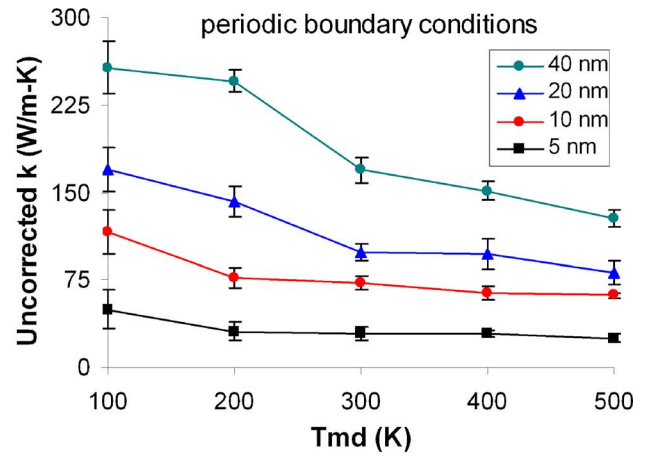
Fig. 2 Uncorrected thermal conductivity versus temperature at different nanotube lengths for (10, 10) SWNTs with both: (a) free; and (b) periodic boundary conditions

the $S\Delta t$ product in Eq. (11). The effect of neglecting $S\Delta t$ is to remove the effects of total (classical) lattice energy and number of atoms, so that different domain sizes and temperatures can be compared using axes with the same scales. This convention is also followed here for all DOS plots. Figure 1 shows the longitudinal phonon DOS (arbitrary units) at 300 K for (10, 10) SWNTs with two different lengths and two different boundary conditions. Four thousand temporal points are used in calculating the density of states. Therefore the spectral resolution is 0.25 THz. All graphs have a strong peak around 52 THz, which is characteristic of the two-dimensional (2D) graphene sheet phonon spectrum [38]. In all plots with free boundaries, there is also a strong low-frequency peak. This peak is absent in PBC cases. The physical meaning of the peak is that there is an additional vibrational mode not present in the PBC tubes, which represents the periodic axial oscillation of the free tube ends. Dickey and Paskin [39] found a similar low frequency mode for small particles with free surfaces. The peak appears at 1.25 THz, 0.75 THz, 0.5 THz, and 0.25 THz at nanotube lengths 5 nm, 10 nm, 20 nm, and 40 nm, respectively. The reduction in peak position with tube length does not scale linearly; this is likely a result of the 0.25 THz resolution. The resolution can be increased by using significantly longer simulation times; however, such times are computationally intensive and beyond the scope of the present study.

The full DOS was also calculated. This was done by replacing the product of axial velocity components in Eq. (11) with the dot product of velocities

$$D_{\text{full}}(\omega) = S \int dt\, e^{-i\omega t} \langle \vec{v}(t) \cdot \vec{v}(0) \rangle = S\Delta t \cdot \text{FFT}[\langle \vec{v}(t) \cdot \vec{v}(0) \rangle]$$

(12)

Unlike the clear "peak" / "no peak" behavior of the longitudinal density of states, the full density of states shows a low-frequency peak for both PBC and free cases that is more pronounced with free boundary conditions. The inclusion of radial and tangential velocity components in the full DOS (Eq. (12)) contributes additional vibrational modes and it is likely that these partially obscure any "peak"/"no peak" effect occurring at low frequencies.

Temperature Dependence and Quantum Correction. For both free boundary and PBC cases, thermal conductivity monotonically decreases with increasing temperature as shown in Fig. 2. This temperature dependence disagrees with the available low-temperature ($<$500 K) experimental data. The reason for this disagreement is that quantum effects, which are important at temperatures below the Debye temperature, are completely neglected in the classical MD approach. Thus, quantum corrections to the MD calculations of temperature and thermal conductivity are necessary. Temperature in MD simulations (T_{MD}) is typically calculated based on the mean kinetic energy of the system. By assuming that the total system energy is twice the mean kinetic energy at T_{MD} (equipartition) and equal to the total phonon energy of the system at the quantum temperature T, correction is made through [40]

$$m\sum_{i=1}^{N} \vec{v}_i \cdot \vec{v}_i = 3Nk_B T_{\text{MD}} = \int_0^{\omega_{\max}} D_{\text{tot}}(\omega)\left[\frac{1}{(e^{\hbar\omega/k_B T} - 1)} + \frac{1}{2}\right]\hbar\omega\, d\omega$$

(13)

where $D_{\text{tot}}(\omega)$ is the phonon density of states summed over all acoustic branches and the $\frac{1}{2}$ term represents the effect of zero point energy. Essentially, this procedure corrects for the low-temperature heat capacity variation with temperature that is not accounted for in the classical simulation. It provides a means for mapping results calculated classically onto their quantum analogs at the same energy level.

To implement the quantum correction here, the Debye density of states [41] is used. On a per atom basis and converting from angular frequency to frequency Eq. (13) becomes

$$T_{\text{MD}} = \frac{1}{3k_B}\int_0^{\nu_D} b_{\text{tot}}(\nu)\left[\frac{1}{(e^{h\nu/k_B T} - 1)} + \frac{1}{2}\right]h\nu\, d\nu$$

(14)

The total DOS is the sum over the longitudinal, two degenerate transverse, and twist densities of states

$$b_{\text{tot}} = b_{\text{LA}} + 2b_{\text{TA}} + b_{\text{TW}} = \frac{4\pi\nu^2}{\left(\frac{N}{V}\right)}\left(\frac{1}{c_{\text{LA}}^3} + \frac{2}{c_{\text{TA}}^3} + \frac{1}{c_{\text{TW}}^3}\right) = 4\left[\frac{4\pi\nu^2}{c_{\text{av}}^3\left(\frac{N}{V}\right)}\right]$$

(15)

and $c_{\text{av}} = 11.26$ km/s is the speed of sound averaged over the four branches according to their weights in the density of states. The velocities of the individual branches are given as $c_{\text{LA}} = 20.35$ km/s, $c_{\text{TA}} = 9.43$ km/s, and $c_{\text{TW}} = 15$ km/s [8]. The upper limit of Eq. (14) is the Debye frequency, which scales with Debye temperature through the proportionality factor k_B/h. It is not entirely clear what the correct Debye temperature value is for carbon nanotubes, but it is expected to be similar to that of graphite [8]. Several studies quote or estimate high values

for graphite, e.g., >2000 K [8] and 2500 K [42]. A recent first-principles study of graphite [43] reveals a temperature dependent Debye temperature: ~400 K at 0 K rising dramatically to ~1900 at high temperature. It is important to note that dramatically different Debye temperatures are often quoted for different modes in the same material, for example 2100 K for longitudinal modes versus 614 K for transverse modes propagating in-plane in graphite [44]. In other cases a single value, determined from fitting experimental heat capacity data or from DOS calculations that average among the various vibrational modes, is reported. The latter approach is used here (Eq. (15)). The Debye frequency is found from the number of modes in a single acoustic branch, which is equal to the number of primitive cells in the domain [41] and also to the number of atoms divided by the number of basis atoms per primitive cell p

$$M = \frac{N}{p} = \int_0^{\nu_D} D_{av}(\nu) d\nu = \int_0^{\nu_D} \frac{N b_{tot}(\nu)}{4} d\nu = \int_0^{\nu_D} \frac{4N\pi\nu^2}{c_{av}^3 \left(\frac{N}{V}\right)} d\nu \tag{16}$$

with the Debye frequency evaluated from the integral as

$$\nu_D = c_{av} \left[\frac{3\left(\frac{N}{V}\right)}{4\pi p} \right]^{1/3} = \frac{k_B T_D}{h} \tag{17}$$

The Debye frequency, using the average branch speed c_{av} and assuming the cross-sectional area of the nanotube is a ring of van der Waals thickness 3.4 Å, is 9.86 THz. The corresponding Debye temperature, 473 K, is comparable to reported values of 475 K [45] and 580 K [46]. It should be noted that our value is lower than other reported values for nanotubes such as 960 K [9], 1000 K [47], and the ~2000 K values reported for graphite. These differences may arise from the different treatments of the density of states used (e.g., Refs. [9,47]) or possibly from the use of longitudinal instead of averaged phonon velocity. Regardless, the use of a "low" Debye temperature will give a conservative estimate of the quantum correction, which is why it has been used here.

The relation between T_{MD} and T obtained from Eq. (14) is shown in Fig. 3(a). T_{MD} and quantum temperature T differ at low temperature but approach one another at high temperature. This is more clearly illustrated in Fig. 3(b), which shows the temperature dependence of dT_{MD}/dT. In this figure the slope approaches 1 as temperature increases. Inclusion of the zero point energy in Eq. (14) results in a corresponding "zero point temperature": an MD temperature below which there is no classical analog to any quantum temperature.

The quantum correction is incorporated in the thermal conductivity expression by multiplying the thermal conductivity in Fourier's law by a factor dT_{MD}/dT [48]

$$k_{qc} = -\frac{q_z}{dT/dz} = -\frac{q_z}{(dT/dT_{MD})(dT_{MD}/dz)} = \left(\frac{dT_{MD}}{dT}\right) k \tag{18}$$

This calculation reflects that the thermal conductivity directly calculated from MD (k) differs from the quantum corrected thermal conductivity (k_{qc}) due to the differing classical and quantum definitions of temperature. It is evident from Eq. (18) and Fig. 3(b) that the quantum correction is largest at low temperature and is negligible at high temperature.

The corrected thermal conductivities are shown in Fig. 4. They should be viewed as qualitative in nature due to the assumptions of Debye density of states, definition of nanotube cross-sectional area, and averaged velocity that have been used. Corrections have not been applied to the $T_{MD}=100$ K values since they are below the zero point temperature. In general, the corrected thermal conductivities are lower than the uncorrected (classical) thermal conductivities. The difference between quantum corrected and classi-
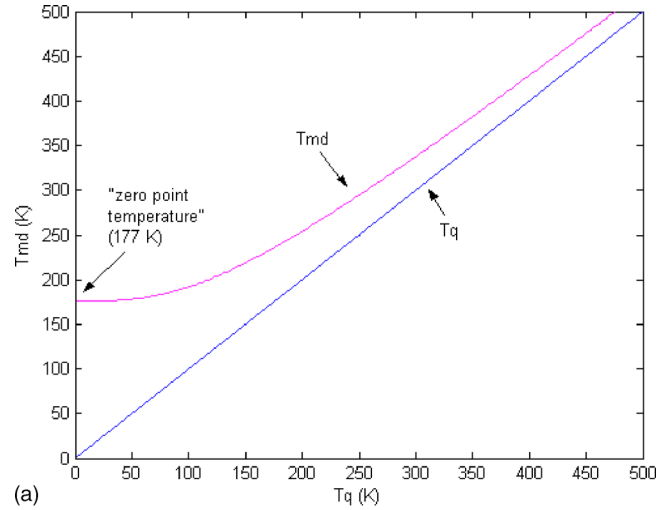
(a)
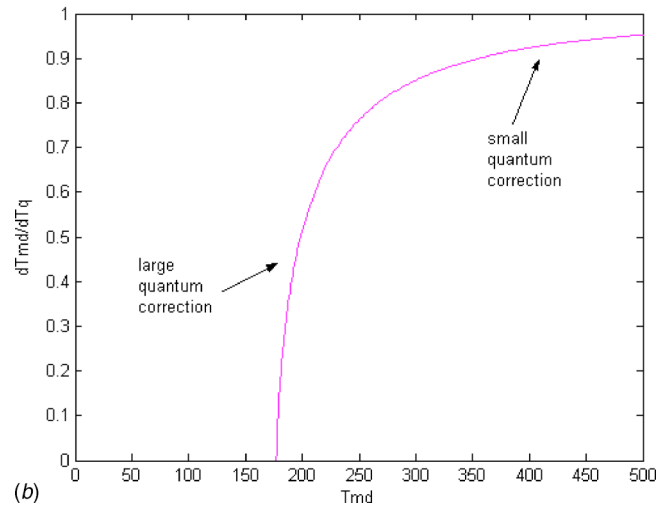
(b)

Fig. 3 (*a*) **MD temperature versus quantum temperature for (10, 10) SWNTs; and (*b*) ratio of MD to quantum temperature versus MD temperature**

cal thermal conductivities decreases with increasing temperature, as is expected from Fig. 3. Unlike the uncorrected results, which monotonically decrease with temperature, the corrected results display a slight increase with temperature to a maximum value at ~400 K, then a slight decrease. This trend is consistent with thermal conductivity measurements for single-wall carbon nanotubes [5] and multiwall carbon nanotubes [2,3] and is also consistent with the Debye temperature calculated above. The use of a higher Debye temperature/frequency yields a stronger correction due to inclusion of higher frequency modes; these modes are more quantum in nature [33]. This results in a sharper peak and lower values than in Fig. 4 but qualitatively the results are similar, as ascertained from another set of simulations run at a higher Debye temperature. It is questionable that some other studies [16,17] using classical MD simulations can also attain this peaking behavior without a quantum correction, as $k \sim 1/T$ temperature dependence is expected in the purely classical regime. We agree with Maruyama [22] that these studies are likely suffering from artifacts of small simulation cell size, which cuts off long wavelengths at lower temperatures and thus artificially reduces the low-temperature thermal conductivity.

Effect of Boundary Conditions. Figures 2 and 4 illustrate that thermal conductivity in nanotubes with free boundaries is lower
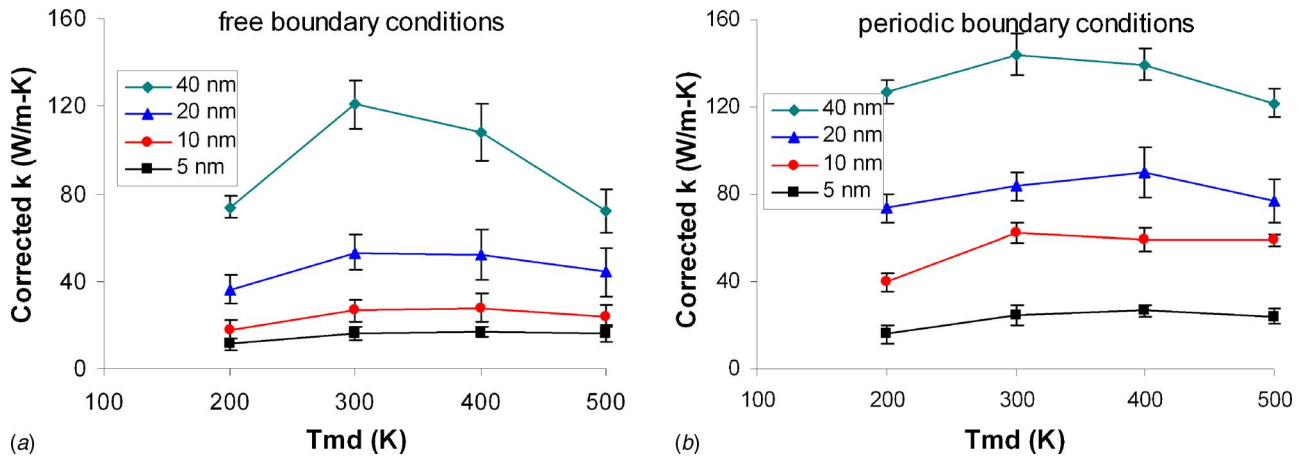
Fig. 4 Estimated values of quantum corrected thermal conductivity versus temperature at different nanotube lengths for (10, 10) SWNTs with both: (a) free; and (b) periodic boundary conditions

than that with periodic boundary conditions. The effect of the free boundary is to reduce the phonon lifetime due to additional scattering at the tube ends, which reduces the correlation of heat flux vector at time t with the initial heat flux vector. This reduction is very strong in the 5 nm tubes. In Fig. 5(a) it is seen that the HCACF decays to zero very quickly and then fluctuates about this value, which leads to much lower thermal conductivity compared to that of the PBC case (Eq. (2)). With increasing tube length the effect of boundary scattering is less severe, as indicated in Fig. 5(b) for the 40 nm free boundary case. The HCACF curve starts to have a long decaying tail and becomes similar to that of the PBC. For all PBC simulations and for free simulations of 20 nm or longer, the HCACF has a fast decay followed by a longer decay. In general, HCACF in PBC nanotubes decays more slowly than those with free boundary conditions, which leads to higher thermal conductivity. For both cases, HCACF decays more slowly with increasing length, leading to a length dependent thermal conductivity.

It is also evident in Fig. 5 that there are pronounced high-frequency oscillations for the free boundary condition cases as compared to the PBC cases. This is believed to arise from the dangling carbons at the free ends, whose vibrations contribute strongly to the periodic reversals of the heat current.

Phonon Decay Times. For the thermal conductivity calculations described above, the phonon decay times τ_1 and τ_2 were

calculated based on double exponential fits to the free and PBC nanotube HCACF before the ballistic transport time τ_b. Although this "early time" fitting was a requirement for the PBC nanotubes, it was only done for the free nanotubes to provide a consistent basis for comparison to the free case. Free nanotubes require no such time truncation, so HCACF fits were also performed for much longer times, up to 100 ps, to see the effects of fitting time. The overall time constants were not observed to change significantly for the fitting times investigated, although as expected the 100 ps fits resulted in the lowest fitting errors.

Results for τ_2 from the 100 ps HCACF fitting are shown in Fig. 6 for nanotubes with free boundary conditions, and the corresponding results for τ_1 are found in Table 2. For PBC nanotubes it was not possible to perform reasonable 100 ps fits for τ_1 and τ_2 directly due to the spurious self correlation effects that appeared much earlier than this time. From Fig. 6 it is clear that τ_2 for nanotubes with free boundaries increases linearly with nanotube length and increases as temperature decreases. These phenomena can be understood from Matthiessen's rule

$$\frac{1}{\tau_{2,\text{free}}} = \frac{1}{\tau_{p-p}} + \frac{2}{\tau_b} = \frac{1}{\tau_{p-p}} + \frac{2c}{L} \qquad (19)$$

Here the overall scattering rate for the free nanotube $1/\tau_{2,\text{free}}$ is determined by the characteristic times for phonon–phonon scattering, τ_{p-p}, and boundary scattering, τ_b. Note that τ_b is the same as
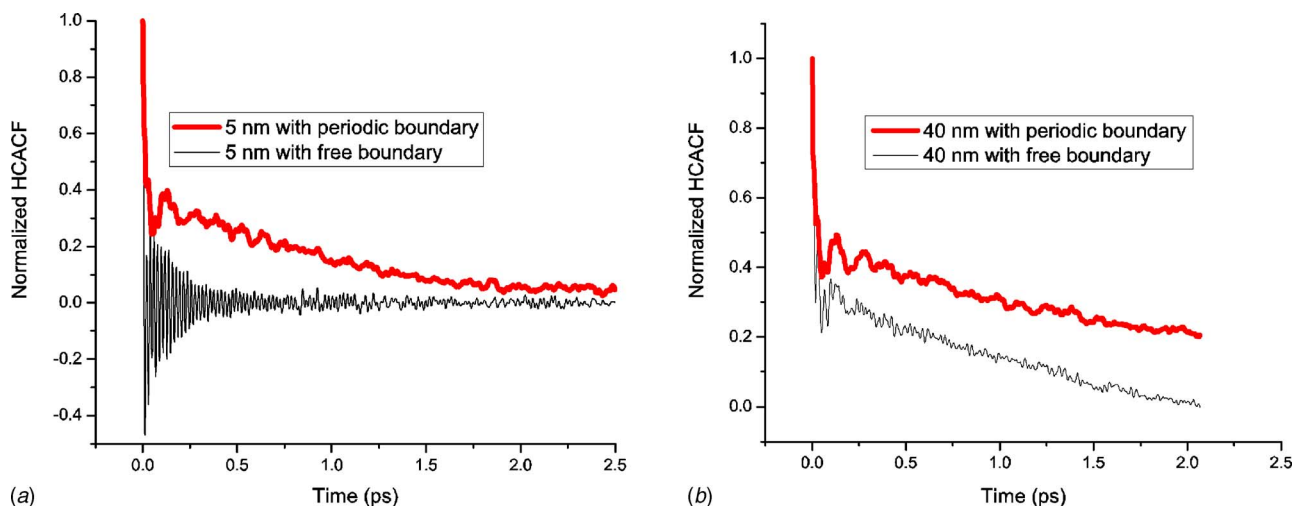

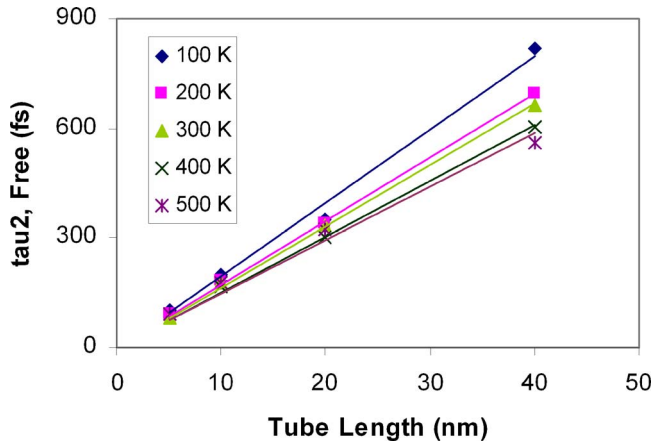**Fig. 5 Normalized HCACF for (a) 5 nm, and (b) 40 nm (10, 10) SWNTs at $T_{\text{MD}} = 300$ K**

Fig. 6 Time constant τ_2 versus length at different temperatures (T_{MD}) for (10, 10) SWNTs with free boundary conditions

Table 3 Apparent (10,10) carbon nanotube speed of sound (m/s) estimated from Fig. 6 and Eq. (23) at different temperatures (T_{MD})

100 K	200 K	300 K	400 K	500 K
25,100	28,800	30,041	32,900	34,100

the ballistic transport time. Similar approaches have been used to account for finite size effects on phonon mean free path in MD simulations [49,50]. The $\tau_b/2$ represents the average time a phonon has traveled (one-dimensional geometry) since last scattering from either end of the nanotube

$$\tau_{av} = \frac{l}{c} = \frac{\int_0^L z\,dz}{c\int_0^L dz} = \frac{L}{2c} = \frac{\tau_b}{2} \qquad (20)$$

Equation (19) shows that as length increases, $\tau_{2,free}$ also increases. This increase is linear when $\tau_{av} \gg \tau_{p-p}$, leading to

$$\tau_{2,free} \approx \tau_{av} = \frac{L}{2c} \quad \text{(ballistic regime)} \qquad (21)$$

The linear increase in Fig. 6 thus indicates that the observed nanotubes are in the ballistic transport regime: nanotube lengths are much shorter than the phonon mean free path l in this regime. The decrease in $\tau_{2,free}$ as temperature increases indicates that the transport, although still largely ballistic, is moving toward the diffusive end of the ballistic–diffusive continuum. This is supported by Eq. (19) and by the well known $\tau_{p-p} \sim 1/T$ temperature dependence in the classical regime. Assuming that the kinetic theory proportionality of thermal conductivity and phonon scattering time

$$k = \rho Ccl = \rho Cc^2 \tau_{p-p} \qquad (22)$$

holds, this behavior is also consistent with the linear dependence of thermal conductivity on length found in Ref. [24]. From Eq. (19) it is evident that as temperature increases, τ_{p-p} decreases and the diffusive phonon–phonon scattering term $1/\tau_{p-p}$ in the denominator becomes larger. At high enough temperatures it will become dominant, leading to fully diffusive transport, which is characterized by no length dependence (i.e., convergence).

In the fully ballistic limit the speed of sound may be estimated from

Table 2 Fast decay time constant τ_1 (in fs) for nanotubes with free boundaries at different lengths and temperatures (T_{MD})

	100 K	200 K	300 K	400 K	500 K
5 nm	4.02	4.098	4.116	4.182	4.249
10 nm	3.834	3.506	4.16	4.377	4.41
20 nm	3.936	4.225	4.566	4.59	5.585
40 nm	4.507	5.205	5.733	6.123	7.08

$$c \approx \frac{L}{2\tau_{2,free}} \quad \text{(ballistic regime)} \qquad (23)$$

Applying this to the reciprocals of the slopes in Fig. 6 yields the results in Table 3. The apparent speed of sound magnitudes range from 25 to 34 km/s as temperature increases from 100 to 500 K. These values are comparable to the 20 km/s L_{LA} value in Ref. [8], but the increase with temperature requires some discussion. Equation (23) is only truly valid when $\tau_{p-p} \to \infty$, which occurs as $T \to 0$. The apparent speed of sound calculated at higher temperatures is too large since $\tau_{2,free}$ is reduced from the ballistic value by the increasing effects of diffusive phonon–phonon scattering. Thus, Eq. (23), taken in the low-temperature limit, provides a simple estimate of the speed of sound that is much easier to use than conventional calculations based on the dispersion relation.

In general, the free nanotube fast decay times τ_1 in Table 2 increase slightly with temperature and nanotube length, ranging between 4 fs and 7 fs for the various cases considered. These local decay times are typically associated with half the vibration period of the carbon–carbon bond, which is in general a length and temperature independent quantity. Using the 52 THz C–C vibration found in Fig. 1 yields a τ_1 value of 9.6 fs, which is a factor of ~2 higher than the τ_1 values in Table 2. The slight length and temperature dependences observed in the table are likely due to minor fitting errors. The reason for the low τ_1 values for free nanotubes is not fully understood but may be an artifact of the pronounced high-frequency oscillations in the HCACF decay in the free boundary cases. It is likely that the double exponential fit samples only the initial, overly steep high frequency decay for τ_1 rather than the time averaged decay over several oscillations. This is supported by the fact that PBC "early time" autocorrelation data, which did not exhibit pronounced high-frequency oscillations, were fitted by a double exponential to yield τ_1 values in the range 8.4–11.7 fs that match the C–C vibration value well. From visual analysis of Fig. 5, it is evident that fitting an envelope to the peaks and valleys of the autocorrelation decay for free boundary cases yields a slower decay approximately equal to both the C–C and PBC "early time" τ_1 values.

Length Dependence of Thermal Conductivity. With increased system size, thermal conductivity is increased for both free and PBC cases shown in Fig. 7. This is consistent with the length dependence found by others [18,20–22,24]. Since the longest tube length modeled here is 40 nm, the thermal conductivity is still far from its ultimate bulk value. The thermal conductivity value is 158 W/m K for a 40 nm tube at 300 K. This is similar to the ~160 W/m K at 61.5 nm length value reported in Ref. [20] and somewhat lower than the 215 W/m K at 50 nm length value reported in Ref. [21]. A significant question that arises is: why does thermal conductivity of the PBC cases increase with length, since there are no free ends and thus no boundary scattering should occur?

The length dependence of thermal conductivity is not a simulation artifact but rather is a real physical effect arising both from the boundary scattering effects discussed above (Eq. (19)) and from the vibrational modes in the nanotube. Longer nanotubes allow additional vibrational modes, and each mode created by increasing the nanotube length provides a new channel for heat transport. Thus, the *heat capacity* increases with length. However, thermal conductivity is proportional to heat capacity per unit vol-
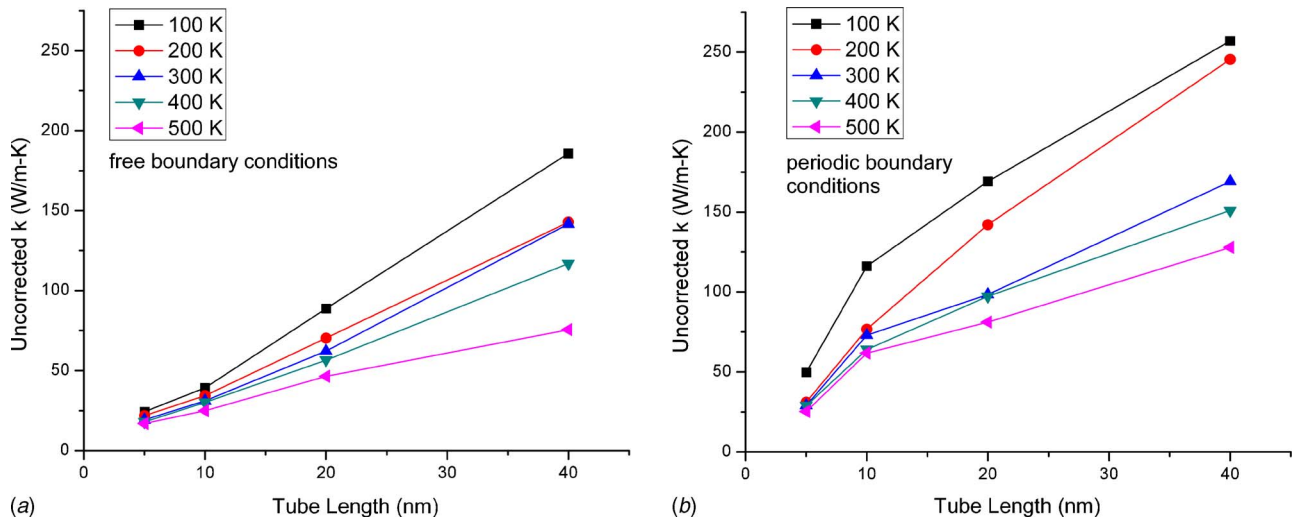
Fig. 7 Uncorrected thermal conductivity versus length at different temperatures (T_{MD}) for (10, 10) SWNTs with both: (*a*) free; and (*b*) periodic boundary conditions

ume ρC, which does not increase with length. So, something else must be responsible for the length dependence of thermal conductivity in PBC nanotubes. Two explanations come to mind. First, the additional modes allowed by the longer nanotubes have smaller wave vectors. Modes with low wave vector have a lower probability of Umklapp scattering, and thus are more long lived than the already existing higher frequency modes. When included with these modes, the net effect is to increase the overall relaxation time and thermal conductivity. Additionally, the results of a recent study [51] indicate that normalized phonon density of states of (10,10) nanotubes does display some length dependence. Briefly, the frequency distribution does not remain constant with increases in length, but instead a redistribution toward lower frequencies occurs. Generally the lower frequencies have higher group velocities which, along with Eq. (22), might explain the observed increase in PBC thermal conductivity with length. It is possible that the length dependence arises as an artifact of the artificial self-correlation that occurs as the phonon circles the simulation cell multiple times. Such correlation effects would be likely to decrease with length as the simulation cell dimension approaches and then exceeds the phonon correlation length, so are not likely to contribute to the observed increase in thermal conductivity with length.

Homogeneous Nonequilibrium Molecular Dynamics. To determine the effect of MD simulation method on calculated thermal conductivity, the homogeneous NEMD method was applied to 5 nm and 10 nm SWNTs with PBC at 300 K. A perturbing force $\vec{F}_e$ was applied in the axial direction with magnitudes ranging from 0.05 to 0.4, the resultant heat current components $J_z(\vec{F}_e,t)$ were calculated, and $k(\vec{F}_e)$ was found using Eq. (5). A plot of perturbed thermal conductivity versus magnitude of perturbing force is shown in Fig. 8. Also shown in Fig. 8 for comparison are thermal conductivity values and data points read from a similar plot from Berber et al. [16]. Note that these data are for a 2.5 nm nanotube at 100 K; Ref. [16] does not provide perturbed thermal conductivity versus magnitude of perturbing force plots at other temperatures or nanotube lengths.

A fit to these data points is required in order to estimate the macroscopic (unperturbed) thermal conductivity $k(\vec{F}_e=0)$. As there is no unambiguous choice for the fitting function in the literature, two types of fits have been chosen: a $1/x$ type fit, which appears to be the type employed by Berber et al., and an exponential fit. The functional forms of the fits are $k(\text{Fe})=a/(\text{Fe}-b)$

and $k(\text{Fe})=A_1 \exp(-\text{Fe}/t_1)$, each with two fitting parameters (Table 4). The $1/x$ fit is shifted along the abscissa by the amount b in order to allow extrapolation to a finite macroscopic conductivity. A simple power law fit $y=a/x$ is not used because extrapolation to zero $\vec{F}_e$ gives an unphysical infinite thermal conductivity.

Extrapolation to zero $\vec{F}_e$ by the exponential fit gives thermal conductivities 233 W/m K for 5 nm and 240 W/m K for 10 nm SWNT at 300 K, and using the $1/x$ fit gives 345 W/m K for 5 nm and 375 W/m K for 10 nm (Fig. 4). These values are significantly higher than the corresponding values calculated in this paper by the EMD method (73 W/m K for EMD with PBC for 10 nm SWNT at 300 K), but still much lower than the 300 K value of 6600 W/m K reported in Ref. [16]. To explain the discrepancy with Berber et al.'s value, we have fit their available (100 K, 2.5 nm) data points using both exponential and $1/x$ type fits. We were unable to reproduce their 100 K value of 37,000 W/m K. Our exponential fit to their data yielded a value of about 235 W/m K, which is similar to our exponential fitting
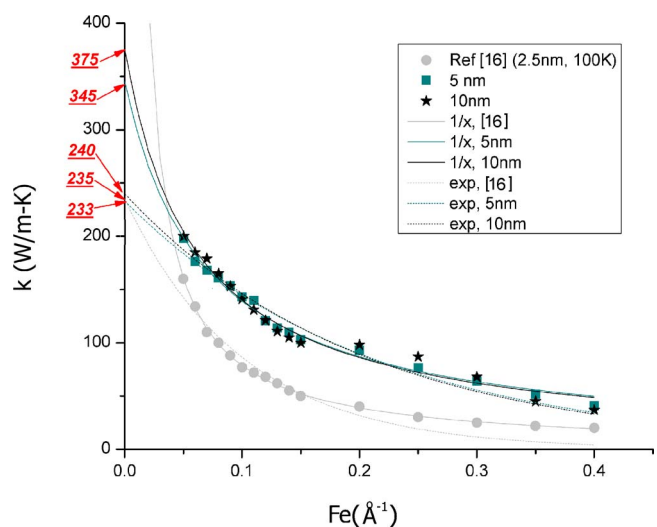

Fig. 8 Perturbed thermal conductivity versus perturbation (**Fe**) calculated by homogeneous molecular dynamics simulation at T_{MD}=300 K. Macroscopic thermal conductivity values for the various cases are underlined.

Table 4 Fitting parameters and macroscopic thermal conductivities from homogeneous nonequilibrium molecular dynamics

	1/x fit			Exponential fit		
	Macroscopic thermal conductivity (W/m K)	a (W/m K Å^{-1})	b (Å^{-1})	Macroscopic thermal conductivity (W/m K)	A_1 (W/m K)	t_1 (Å^{-1})
5 nm	**345**	23.3	−0.0675	**233**	233	0.210
10 nm	**375**	22.3	−0.0595	**240**	240	0.202
Ref. 16 (2.5 nm, 100 K)	**undefined**	7.72996	0.00171	**235**	235	0.0999

values for 5 nm and 10 nm nanotubes at 300 K, while the 1/x type fit did not yield any value as the fitted curve never intercepted the y axis. The influence of error in reading data from the plot was investigated by incorporating small changes in the obtained data points and observing the resultant change in fitting parameters and conductivity. No significant changes were observed; the exponential fit macroscopic thermal conductivity changed by <5% and the 1/x fit conductivity was still undefined. So, it is unlikely that the discrepancies between the present results and those in Ref. [16] are due to misreading of the published data.

The overall error in the exponential fit values for 5 nm and 10 nm nanotubes is about 4%, while that of the 1/x fit is about 13%. The macroscopic thermal conductivity values for 5 nm and 10 nm nanotubes differ by less than this error, so no clear length effect can be determined from the HNEMD data points. The 1/x and exponential fits differ by about 35%, with the 1/x fit consistently higher than the exponential fit. This difference may be taken as a rough estimate of the uncertainty in the values obtained by HNEMD.

Comparison to Literature Values. Although extrapolation using different fitting functions will result in different thermal conductivity values from homogeneous NEMD, it is not clear how the presented k versus Fe data in Berber's paper could be extrapolated to yield a 100 K thermal conductivity value of 37,000 W/m K. This also brings into question the value of 6600 W/m K reported at 300 K. Moreland et al. [21], Maruyama [22], and recently Padgett and Brenner [20] all used direct NEMD and found similar conductivity values, despite using different potentials and boundary conditions. Results in the present paper for both EMD and homogeneous NEMD cases are similar to those in the above three papers but are much smaller than that from Che et al. [18] who used EMD and the same boundary conditions. The only difference is the potential, REBO versus Tersoff–Brenner, which did not appear to play a significant role in the three direct NEMD simulations above. The reason for the difference between Che's and the present data are thus still not clear, although scaling by the same cross-sectional area reduces the discrepancy to a factor of ~5. It is possible that the precise procedure used in the autocorrelation decay calculation and fitting process in Ref. [18] may also play some role, but these details are not provided so no definitive statement can be made. Osman et al. [17] used the same NEMD and heat flux control technique as Padgett and Brenner [20] but got much higher values. At present, these discrepancies are also not understood, unless they are a result of stress or some other unknown factor.

The earlier thermal conductivity results in Table 1 show considerable scatter and have not been replicated by other groups. The more recent results, including those of the present paper, are all on the order of a few hundred W/m K for the tube lengths considered. Due to the consistency found in these later results, it is believed that these are more likely to be correct than the earlier values. This is confirmed by Mingo and Broido [24] who found about 100 W/m K for a 100 nm (10, 0) SWNT at 316 K. Although the temperature and chirality are different, the order of

magnitude is the same. The ultimate test of correctness is, however, similarity to experimental data. The "correct" simulations in Table 1 are an order of magnitude lower than available experimental data, but are also performed on tubes that are short (most are less than a few hundred nm) relative to the expected experimental lengths of a few microns in order to enable comparison of a variety of papers. Simulations on longer tubes (400 nm [22] and 1000 nm [21]) indicate that thermal conductivity has still not converged and will continue to increase with tube length. This behavior is expected due to the long phonon mean free path and is a likely reason for the low "correct" values. This indicates that calculated values approaching experimental values may be attainable for simulations performed on sufficiently long tubes. Additionally, HNEMD yields values a factor of 3–12 higher than EMD PBC results calculated for the same tube length. Detailed discussion of the differences among the various simulation methods is the subject of another publication [51]. It remains to be seen whether differences in intermolecular potential will have a significant effect at longer tube lengths.

Conclusions

Using molecular dynamics simulations we have calculated the thermal conductivity for (10, 10) single-wall carbon nanotubes as a function of temperature, length, and simulation method for both free boundary and periodic boundary conditions. To qualitatively account for the quantum effect, a correction is made to the thermal conductivity. The corrected values increase with increasing temperature and fall off at high temperature, showing a trend that is consistent with experimental observations. The free boundaries reduce phonon lifetime due to additional phonon scattering at tube ends and therefore give lower thermal conductivity than that of periodic boundary conditions. Thermal conductivity increases with length at all temperature and boundary conditions. Linear increases in τ_2 and monotonic increases in thermal conductivity indicate ballistic transport in these simulations, and provide a simple means to estimate phonon speed of sound. An uncorrected value of about 160 W/m K is found at 300 K for a 40 nm tube length using equilibrium molecular dynamics. Homogeneous nonequilibrium molecular dynamics simulation indicates a factor of 3–12 increase as compared to equilibrium molecular dynamics with periodic boundary conditions for nanotubes at 300 K. The present results agree well with recent theoretical results for carbon nanotube thermal conductivity, which are consistent with each other at comparable nanotube lengths. Discrepancies between simulated and experimental values are attributed to length effects, and may also arise due to the effects of simulation method, stress, and intermolecular potential.

Nomenclature

b = density of states per atom
C = heat capacity (per unit mass)
c = speed of sound
D = density of states (states/frequency)
ε = atomic energy including both potential and kinetic
EMD = equilibrium molecular dynamics
$\vec{f}_{ij}$ = force on atom i due to atom j
$\vec{F}_e$ = external force field in homogeneous NEMD
$\vec{F}_i$ = total force on atom i
HCACF = heat current autocorrelation function
HNEMD = homogeneous nonequilibrium molecular dynamics
$h, \hbar$ = Planck's constant, Planck's constant divided by 2π
J = heat current
k = thermal conductivity (axial direction)
k_B = Boltzmann's constant
L = nanotube length
l = phonon mean free path
m = atomic mass
M = number of primitive cells in simulation domain
MD = molecular dynamics
MWNT = multi-wall carbon nanotube
N = number of atoms
NEMD = nonequilibrium molecular dynamics
p = number of basis atoms per primitive cell
PBC = periodic boundary conditions
r_{ij} = distance between atom i and j
$\vec{r}$ = atomic position vector
REBO = reactive bond order potential
SWNT = single-wall carbon nanotube
S = scale factor in density of states
q = heat flux
T, T_q = (quantum) temperature
T_{MD} = MD temperature
Δt = MD simulation timestep
t_{corr} = correlation time
t_{run} = simulation run time
TB = Tersoff–Brenner potential
$\vec{v}$ = atomic velocity vector
V = volume of nanotube

Greek

ν = frequency
ν_D = Debye frequency
ρ = mass density
τ_1, τ_2 = time constant in double exponential fit for HCACF
τ_b = boundary scattering time
τ_{p-p} = phonon–phonon scattering time
ω = angular frequency
$\vec{\omega}$ = angular velocity of simulation system
σ_k = probable error of thermal conductivity
σ_T = probable error of temperature
$\sigma_{\langle J(t)J(0)\rangle}$ = probable error of HCACF
$\langle\rangle$ = average

Subscripts

acoustic = acoustic modes
av = averaged over all four acoustic modes
D = Debye
i, j, k = summation index, atom index
free = free boundary condition
full = full
LA = longitudinal acoustic mode
long = longitudinal
max = maximum angular frequency in density of states
PBC = periodic boundary condition
qc = quantum corrected
TA = transverse acoustic mode
tot = total density of states
TW = twist acoustic mode
z = axial direction

References

[1] Hone, J., Whitney, M., Piskotti, C., and Zettl, A., 1999, "Thermal Conductivity of Single-Walled Carbon Nanotubes," Phys. Rev. B, **59**(4), pp. R2514–R2516.

[2] Kim, P., Shi, L., Majumdar, A., and McEuen, P. L., 2001, "Thermal Transport Measurements of Individual Multiwalled Nanotubes," Phys. Rev. Lett., **87**(21), p. 215502.

[3] Fujii, M., Zhang, X., Xie, H., Ago, H., Takahashi, K., and Ikuta, T., 2005, "Measuring the Thermal Conductivity of a Single Carbon Nanotube," Phys. Rev. Lett., **95**, p. 065502.

[4] Choi, T.-Y., Poulikakos, D., Tharian, J., and Sennhauser, U., 2006, "Measurement of the Thermal Conductivity of Individual Carbon Nanotubes by the Four-Point Three-ω Method," Nano Lett., **6**(8), pp. 1589–1593.

[5] Yu, C. H., Shi, L., Yao, Z., Li, D. Y., and Majumdar, A., 2005, "Thermal Conductance and Thermopower of an Individual Single-Wall Carbon Nanotube," Nano Lett., **5**(9), pp. 1842–1846.

[6] Pop, E., Mann, D., Wang, Q., Goodson, K., and Dai, H., 2006, "Thermal Conductance of an Individual Single-Wall Carbon Nanotube Above Room Temperature," Nano Lett., **6**(1), pp. 96–100.

[7] Haile, J. M., 1992, *Molecular Dynamics Simulation: Elementary Methods*, Wiley, New York.

[8] Dresselhaus, M. S., and Eklund, P. C., 2000, "Phonons in Carbon Nanotubes," Adv. Phys., **49**(6), pp. 705–814.

[9] Hone, J., 2001, "Phonons and Thermal Properties of Carbon Nanotubes," *Carbon Nanotubes, Topics in Applied Physics*, M. S. Dresselhaus, G. Dresselhaus, and P. Avouris, eds., Springer, Berlin, Germany, **80**, pp. 273–286.

[10] Yi, W., Lu, L., Zhang, D.-L., Pan, Z. W., and Xie, S. S., 1999, "Linear Specific Heat of Carbon Nanotubes," Phys. Rev. B, **59**(14), pp. R9015–R9018.

[11] Hoover, W. G., and Ashurst, W. T., 1975, "Nonequilibrium Molecular Dynamics," in *Theoretical Chemistry: Advances and Perspectives*, H. Eyring and D. Henderson, eds., Academic, New York, **1**, pp. 1–51.

[12] Frenkel, D., and Smit, B., 2002, *Understanding Molecular Simulation: From Algorithms to Applications*, 2nd ed., Academic, San Diego, Chap. 3.

[13] Hansen, J.-P., and McDonald, I. R., 1986, *Theory of Simple Liquids*, 2nd ed., Academic, London, Chap. 5.

[14] Irving, J. H., and Kirkwood, J. G., 1950, "The Statistical Mechanical Theory of Transport Processes. IV. The Equations of Hydrodynamics," J. Chem. Phys., **18**(6), pp. 817–829.

[15] Evans, D. J., 1982, "Homogeneous NEMD Algorithm for Thermal Conductivity—Application of Non-Canonical Linear Response Theory," Phys. Lett., **91A**(9), pp. 457–460.

[16] Berber, S., Kwon, Y. K., and Tomanek, D., 2000, "Unusually High Thermal Conductivity of Carbon Nanotubes," Phys. Rev. Lett., **84**, pp. 4613–4616.

[17] Osman, M. A., and Srivastava, D., 2001, "Temperature Dependence of the Thermal Conductivity of Single-Wall Carbon Nanotubes," Nanotechnology, **12**, pp. 21–24.

[18] Che, J., Çagin, T., and Goddard, W. A., III, 2000, "Thermal Conductivity of Carbon Nanotubes," Nanotechnology, **11**, pp. 65–69.

[19] Yao, Z., Wang, J., Li, B., and Liu, G., 2005, "Thermal Conduction of Carbon Nanotubes Using Molecular Dynamics," Phys. Rev. B, **71**, p. 085417.

[20] Padgett, C. W., and Brenner, D. W., 2004, "Influence of Chemisorption on the Thermal Conductivity of Single-Wall Carbon Nanotubes," Nano Lett., **4**(6), pp. 1051–1053.

[21] Moreland, J. F., Freund, J. B., and Chen, G., 2004, "The Disparate Thermal Conductivity of Carbon Nanotubes and Diamond Nanowires Studied by Atomistic Simulation," Microscale Thermophys. Eng., **8**(1), pp. 61–69.

[22] Maruyama, S., 2003, "A Molecular Dynamics Simulation of Heat Conduction of a Finite Length Single-Walled Carbon Nanotube," Microscale Thermophys. Eng., **7**, pp. 41–50.

[23] Mingo, N., and Broido, D. A., 2005, "Carbon Nanotube Ballistic Thermal Conductance and Its Limits," Phys. Rev. Lett., **95**, p. 096105.

[24] Mingo, N., and Broido, D. A., 2005, "Length Dependence of Carbon Nanotube Thermal Conductivity and the "Problem of Long Waves"," Nano Lett., **5**(7), pp. 1221–1225.

[25] Brenner, D. W., 1990, "Empirical Potential for Hydrocarbons for use in Simulating the Chemical Vapor Deposition of Diamond Films," Phys. Rev. B, **42**(15), pp. 9458–9471.

[26] Brenner, D. W., Shenderova, O. A., Harrison, J. A., Stuart, S. J., Ni, B., and Sinnott, S. B., 2002, "A Second-Generation Reactive Empirical Bond Order (REBO) Potential Energy Expression for Hydrocarbons," J. Phys.: Condens. Matter, **14**, pp. 783–802.

[27] Abramson, A. R., Tien, C.-L., and Majumdar, A., 2002, "Interface and Strain Effects on the Thermal Conductivity of Heterostructures: A Molecular Dynamics Study," J. Heat Transfer, **124**(5), pp. 963–970.

[28] Shi, L., 2001, "Mesoscopic Thermophysical Measurements of Microstructures and Carbon Nanotubes," Ph.D. thesis, University of California, Berkeley, CA.

[29] Zhou, Y., Cook, M., and Karplus, M., 2000, "Protein Motions at Zero-Total Angular Momentum: The Importance of Long-Range Correlations," Biophys. J., **79**, pp. 2902–2908.

[30] Goldstein, H., 1980, *Classical Mechanics*, Addison-Wesley, Reading, MA, Chap. 3.

[31] Hoover, W. G., 1985, "Canonical Dynamics: Equilibrium Phase-Space Distribution," Phys. Rev. A, **31**(3), pp. 1695–1697.

[32] Volz, S. G., and Chen, G., 2000, "Molecular-Dynamics Simulation of Thermal Conductivity of Silicon Crystals," Phys. Rev. B, **61**(4), pp. 2651–2656.

[33] Che, J., Çagin, T., Deng, W., and Goddard, W. A., III, 2000, "Thermal Conductivity of Diamond and Related Materials from Molecular Dynamics Simulations," J. Chem. Phys., **113**(6), pp. 6888–6900.

[34] McGaughey, A. J. H., and Kaviany, M., 2004, "Thermal Conductivity Decomposition and Analysis Using Molecular Dynamics Simulations. Part I. Lennard-Jones Argon," Int. J. Heat Mass Transfer, **47**, pp. 1783–1798.

[35] Press, W. H., Teukolsky, S. A., Vetterling, W. T., and Flannery, B. P., 1992, *Numerical Recipes in FORTRAN: The Art of Scientific Computing*, 2nd ed., Cambridge University Press, Cambridge, UK, Chap. 2.

[36] Schelling, P. K., and Keblinski, P., 2003, "Thermal Expansion of Carbon Structures," Phys. Rev. B, **68**, p. 035425.

[37] Allen, M. P., and Tildesley, D. J., 1987, *Computer Simulation of Liquids*, Clarendon, Oxford, UK, Chap. 2.

[38] Sokhan, V. P., Nicholson, D., and Quirke, N., 2000, "Phonon Spectra in Model Carbon Nanotubes," J. Chem. Phys., **113**(5), pp. 2007–2015.

[39] Dickey, J. M., and Paskin, A., 1970, "Size and Surface Effects on the Phonon Properties of Small Particles," Phys. Rev. B , **1**(2), pp. 851–857.

[40] Maiti, A., Mahan, G. D., and Pantelides, S. T., 1997, "Dynamical Simulations of Nonequilibrium Processes-Heat Flow and the Kapitza Resistance Across Grain Boundaries," Solid State Commun., **102**(7), pp. 517–521.

[41] Kittel, C., 1996, *Introduction to Solid State Physics*, 7th ed., Wiley, New York.

[42] Chiu, H.-Y., Deshpande, V. V., Postma, H. W. C., Lau, C. N., Mikó, C., Forró, L., and Bockrath, M., 2005, "Ballistic Phonon Thermal Transport in Multi-walled Carbon Nanotubes," Phys. Rev. Lett., **95**, p. 226101.

[43] Tohei, T., Kuwabara, A., Oba, F., and Tanaka, I., 2006, "Debye Temperature and Stiffness of Carbon and Boron Nitride Polymorphs from First Principles Calculations," Phys. Rev. B, **73**, p. 064304.

[44] Gurney, R. W., 1952, "Lattice Vibrations in Graphite," Phys. Rev., **88**(3), pp. 465–466.

[45] Charlier, A., and McRae, E., 1998, "Lattice Dynamics Study of Zigzag and Armchair Carbon Nanotubes," Phys. Rev. B, **57**(11), pp. 6689–6696.

[46] Benoit, J. M., Corraze, B., and Chauvet, O., 2002, "Localization, Coulomb Interactions, and Electrical Heating in Single-Wall Carbon Nanotubes/Polymer Composites," Phys. Rev. B, **65**, p. 241405(R).

[47] Benedict, L. X., Louie, S. G., and Cohen, M. L., 1996, "Heat Capacity of Carbon Nanotubes," Solid State Commun., **100**(3), pp. 177–180.

[48] Lee, Y. H., Biswas, R., Soukoulis, C. M., Wang, C. Z., Chan, C. T., and Ho, K. M., 1991, "Molecular-Dynamics Simulation of Thermal Conductivity in Amorphous Silicon," Phys. Rev. B, **43**(8), pp. 6573–6580.

[49] Schelling, P. K., Phillpot, S. R., and Keblinski, P., 2002, "Comparison of Atomic-Level Simulation Methods for Computing Thermal Conductivity," Phys. Rev. B, **65**, p. 144306.

[50] Chen, Y., Li, D., Lukes, J. R., Ni, Z., and Chen, M., 2005, "Minimum Superlattice Thermal Conductivity from Molecular Dynamics," Phys. Rev. B, **72**, p. 174302.

[51] Lukes, J. R., and Zhong, H., 2006, "Thermal Conductivity of Single Wall Carbon Nanotubes: A Comparison of Molecular Dynamics Simulation Approaches," *Proceedings of the Thirteenth International Heat Transfer Conference*, Sydney, Australia, August 8–13, NAN-29.